








Highly stabilized fiber Bragg grating accelerometer based on cross-type diaphragm

HEMING WEI,¹  CHANGQUAN ZHUANG,¹ JIAWEI CHE,¹
DENGWEI ZHANG,^{2,8} MENGSHI ZHU,¹  FUFEI PANG,¹
CHRISTOPHE CAUCHETEUR,³  XUEHAO HU,³  JAN NEDOMA,^{4,9}
RADEK MARTINEK,⁵ AND CARLOS MARQUES^{6,7} 

¹Key Laboratory of Specialty Fiber Optics and Optical Access Networks, Joint International Research Laboratory of Specialty Fiber Optics and Advanced Communication, Shanghai University, Shanghai 200444, China

²College of Optical Science and Engineering, Zhejiang University, Hangzhou, Zhejiang 310012, China

³The Electromagnetism and Telecommunication Department, University of Mons, 7000 Mons, Belgium

⁴Department of Telecommunications, VSB – Technical University of Ostrava, Ostrava 70800, Czech Republic

⁵Department of Cybernetics and Biomedical Engineering, VSB – Technical University of Ostrava, Ostrava 70800, Czech Republic

⁶CICECO – Aveiro Institute of Materials, Physics Department, University of Aveiro, 3810-193 Aveiro, Portugal

⁷Department of Physics, VSB – Technical University of Ostrava, Ostrava 70800, Czech Republic

⁸seaskyzdw@zju.edu.cn

⁹jan.nedoma@vsb.cz

Abstract: A fiber Bragg grating (FBG) accelerometer based on cross-type diaphragm was proposed and designed, in which the cross-beam acts as a spring element. To balance the sensitivity and stability, the accelerometer structure was optimized. The experimental results show that the designed device has a resonant frequency of 556 Hz with a considerable wide frequency bandwidth of up to 200 Hz, which is consistent with the simulation. The sensitivity of the device is 12.35 pm/g@100 Hz with a linear correlation coefficient of 0.99936. The proposed FBG accelerometer has simple structure and strong anti-interference capability with a maximal cross-error less than 3.26%, which can be used for mechanical structural health monitoring.

© 2024 Optica Publishing Group under the terms of the [Optica Open Access Publishing Agreement](#)

1. Introduction

Vibration measurements are important in engineering systems as the vibration reveals the health situation and can be used for early warning and diagnosis of faults [1–3]. Typically, most of the vibration could damage the mechanical components, and then it is necessary to develop accelerometers for measuring and analyzing the vibration in the fields of aerospace, rail transportation, and petrochemical industry, etc. [4–8]. Many methods have been utilized for developing accelerometers, which are mostly based on piezoelectric devices and fiber-optic sensors [9–11]. Piezoelectric elements usually pose fabrication and signal attenuation problems because of cabling requirements, which limits their practical application in long-term and long-distance monitoring [12,13]. Fiber-optic sensors allow to alleviate these impairments as they owe light weight, resistance to electromagnetic interference and flexible multiplexing capability [14,15].

Among the fiber-optic sensors for acceleration measurements, fiber Bragg gratings (FBGs) accelerators possess flexible multiplexing capability due to their inherent wavelength-encoded deformation/strain response [8]. There are many kinds of accelerometers based on FBGs, which can be divided into cantilever beam type [16–19], flexible hinge type [20–22], and spring-mass

type [23–27]. The principle of cantilever beam type accelerometers is mainly based on the transferring strain induced by the vibrated cantilever beam as the FBG is bonded to the beam surface, resulting in a wavelength shift proportional to the strain and the vertical acceleration. Basumallick *et al.* proposed a cantilever beam type accelerometer considering the effective distance between the sensor axis and the cantilever neutral axis, which has a high sensitivity of 450 pm/g at a low resonant frequency of only 20 Hz [16]. To improve the strain transfer, Jiang *et al.* proposed a different fiber bonding method to enhance the stretching behavior. A sensitivity of 134.29 pm/g and a relatively flat region from 2 to 60 Hz were obtained [17]. To further improve the stability of the cantilever-based accelerators, Fan *et al.* proposed a circular diaphragm-based cantilever structure where the fiber can be mounted on the beam, which showed a high sensitivity and a relatively broad response range [18]. Compared with the cantilever beam type accelerators, the hinge structure-based accelerators can exhibit strong stability. Qiu *et al.* proposed an FBG accelerometer based on three mass blocks and four flexible hinges with a measuring range and a sensitivity of 50–800 Hz and 29 pm/g, respectively [21]. Yin *et al.* designed an FBG accelerometer based on parallel double flexible hinges with a measurement range up to 200 Hz and a sensitivity of 54 pm/g [22]. It should be noted that the structure of such kind of accelerators is relatively complex, so that the sensor is difficult to be encapsulated. Among the proposed devices, the spring-mass based accelerometers are widely used due to the simple structure and high stability. Generally, it contains a mass block and an elastic element that can be considered as a spring. Liu *et al.* proposed a double diaphragm-based FBG accelerometer with a resonant frequency of 1240 Hz and an acceleration sensitivity of 23.8 pm/g@50 Hz [23]. Zhu *et al.* designed a lantern-shaped elastic metal shell-based dual-FBG accelerometer with a resonant frequency of about 1175 Hz and an average acceleration sensitivity of about 9.4 pm/g in the range of 30–300 Hz [25]. All these structures exhibit high-performance sensing behaviors however, more vibration modes could be generated due to the flexible structures, showing that the stability could be problematic. Additionally, the acceleration sensing range is limited and some structures used dual FBG configurations or complex encapsulations/diaphragms.

In this paper, we propose a highly-stabilized FBG accelerometer based on an elastic cross-type diaphragm. The accelerometer structure was optimized and simulated to obtain a stabilized acceleration structure without sacrificing stability. The resonant frequency and the working range were investigated. The proposed device shows good performances for acceleration measurements, which could bring potential applications in the fields of structural health monitoring.

2. Principle operation of sensor

2.1. FBG sensing principle

FBG is one of the most rapidly developing fiber optic passive devices in recent years. It is a grating that forms a periodic distribution of spatial phases within the fiber core, leading to a narrow band spectrum in reflection [28]. The internal structure of FBG is shown in Fig. 1. When a broad-spectrum light source light transmission passes through the grating area, the light that meets the Bragg wavelength condition will be reflected, which can be expressed as [29]:

$$\lambda_B = 2n_{eff}\Lambda \quad (1)$$

where λ_B is the Bragg wavelength of the FBG, n_{eff} is the effective refractive index of the fiber, and Λ is the grating period. This wavelength shifts when the surrounding conditions such as strain and temperature change, as they can modify grating period length or refractive index of the fiber, which can be expressed as:

$$\frac{\Delta\lambda_B}{\lambda_B} = (1 - \rho_e)\Delta\varepsilon + (\alpha + \xi)\Delta T \quad (2)$$

where $\Delta\lambda_B$ is the FBG center wavelength offset, $\Delta\varepsilon$ is the axial strain, ΔT is the temperature increment, ρ_e is the fiber elastic optical coefficient, α and ξ are the thermal optical coefficient and thermal expansion coefficient of the fiber, respectively. In general, FBG sensors are only directly sensitive to axial strain and temperature changes. Therefore, those complex physical quantities (such as acceleration, displacement and stress) can be indirectly measured by converting them into FBG axial strains by means of special elastic structures.

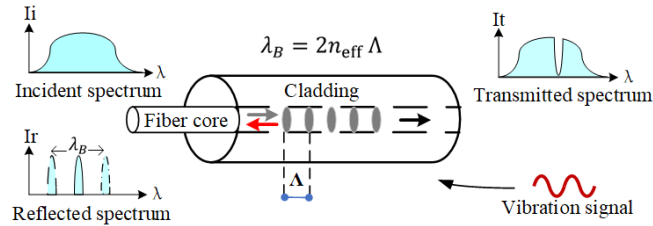


Fig. 1. The principle of FBG sensors.

2.2. Design

An elastic diaphragm based FBG accelerometer is proposed. The structure is schematically shown in Fig. 2, where the elastic diaphragms and the mass blocks are utilized as sensitive elements. Figure 2(a) shows the main design that a mass block is bonded to the central diaphragm and the mass block contains a through-hole allowing the FBG sensor to pass through. The central mass block is connected to the diaphragm periphery by four crossbeams as shown in Fig. 2(b). The elastic diaphragm and mass block are held in the accelerometer center by two box metal cases with screws. The upper and lower box metal shells fix the combination of diaphragm and mass block. The whole constitutes an FBG accelerometer, as shown in Fig. 2(c). Notably, the FBG sensor is located between the mass block and the metal shell below.

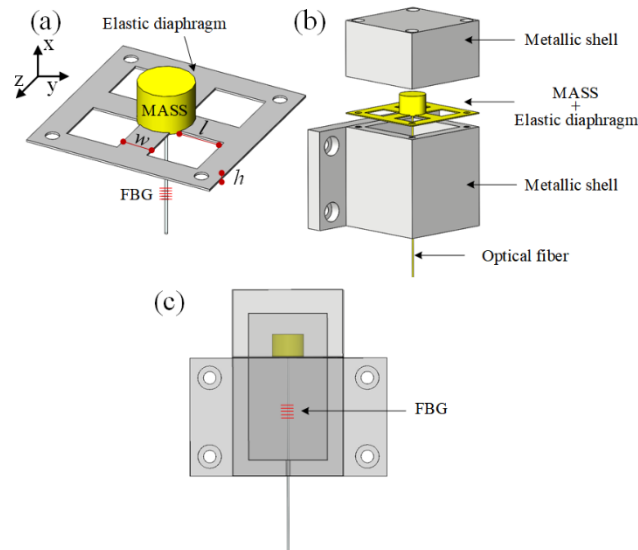


Fig. 2. Accelerometer mechanical structure. (a) Elastic diaphragm and mass block combined structure, FBG one end is fixed inside the mass block. (b) Accelerometer assembly schematic. (c) Accelerometer internal perspective view.

During the response of dynamic vibration, the accelerometer is fixed to the surface of the object to be measured, the vibration displacement can be expressed as $X(t) = x_0 \cos \omega t$, and the relative displacement of the inertial mass block is noted as D . The equation of motion of the system is expressed as [30]:

$$m\ddot{D}(t) + c\dot{D}(t) + kD(t) = m\ddot{X}(t) \quad (3)$$

where m is the mass of the mass block, k is the elasticity coefficient of the spring system, c is the damping coefficient. The steady-state solution of the Eq. (3) is:

$$D(t) = d_0 \cos(\omega t - \theta) \quad (4)$$

where the amplitude d_0 and initial phase θ are given as:

$$d_0 = \frac{x_0(\omega/\omega_n)^2}{\sqrt{[1 - (\omega/\omega_n)^2]^2 + (2\xi\omega/\omega_n)^2}} \quad (5)$$

$$\theta = \tan^{-1} \frac{2\xi\omega/\omega_n}{1 - (\omega/\omega_n)^2} \quad (6)$$

where $\xi = c/2\sqrt{mk}$, $\omega_n = \sqrt{k/m}$, ξ is damping ratio and ω_n is the resonant angular frequency of the system.

From the above analysis, it is clear that the steady-state response is highly nonlinear over the entire range of vibration frequencies, and when the vibration frequency ω is much smaller than the resonant frequency ω_n ($\omega \ll \omega_n$), the special solution of Eq. (3) can be expressed as:

$$D(t) = \frac{1}{\omega_n^2} \omega^2 X_0 \cos(\omega t) \quad (7)$$

This result shows that the relative displacement $D(t)$ of the inertial mass block is proportional to the acceleration $\ddot{X}(t) = -\omega^2 X_0 \cos(\omega t)$ of the excitation signal $X(t)$, thus we can use the structure as an accelerometer when the vibration frequency ω is lower than $\sim 0.2 \omega_n$.

Through the above analysis, we know that the resonant frequency of the system determines the measurement range and sensitivity of the accelerometer, while the resonant frequency is related to m and k . Thus, we need to determine the resonant frequency by adjusting the values of m and k . Crossbeam elasticity coefficient is $k = nEwh^3l^{-3}$, where n is the number of crossbeams, E is the Young's modulus of the diaphragm material, w , h and l are the width, thickness and length of the beam, respectively.

2.3. Simulation and optimization

The proposed structure is numerically studied by the finite element method analysis method. Diaphragm material is chosen from high performance copper alloy QBe2, which has a Young's modulus of 133 GPa with excellent strength, wear resistance and elasticity. Considering that a certain load-bearing capacity of the diaphragm is needed, the diaphragm thickness is set to be 0.3 mm and a mass block has a weight of 7.1 g. Figure 3 shows a vibration mode of the device at a resonant frequency of 636 Hz. To optimize the vibration, the resonant frequencies are simulated as shown in Fig. 4(a). It can be seen that the resonant frequency of the system increases gradually with the increase of w from 1 to 3 mm and the decrease of l from 4.4 to 6 mm. For practical use, an acceleration system with excessively high resonant frequencies, can provide a wide detection range, while resulting in insensitivity at low frequencies. Therefore, it is necessary to design an appropriate resonant frequency for the system based on the actual application requirements.

The simulation results show that multiple diaphragm crossbeam parameters may correspond to the same resonant frequency. To investigate how the sensitivity of the FBG accelerometer is

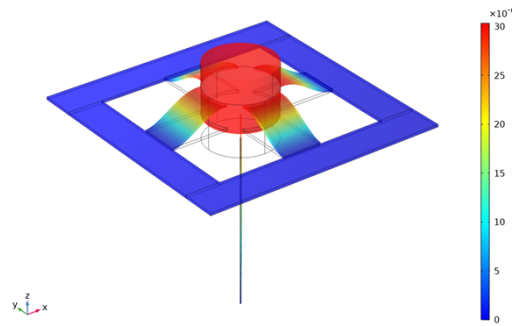


Fig. 3. The vibration mode of the device at a resonant frequency of 636 Hz.

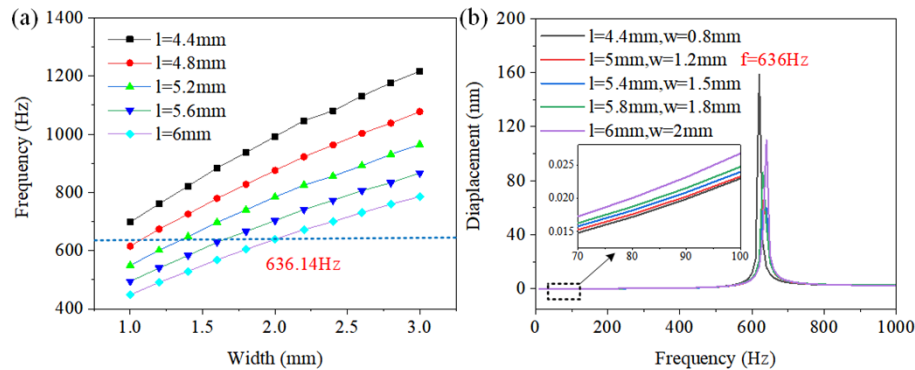


Fig. 4. Elastic diaphragm and mass structure simulation results. (a) Simulation of resonant frequency for different crossbeam widths and lengths. (b) Simulation of the stress sensitivity of the structure at the same resonance frequency with different parameters, the insert is an enlarged picture of part of the area.

related to various crossbeam structure parameters at the same resonant frequency, a resonant frequency of 636 Hz is chosen as shown in Fig. 4(b). It can be seen that the displacement of the mass block increases as the l increases, therefore, the FBG wavelength shifts larger. Considering the size limitation of the accelerometer, the length of the beam is set as $l = 6$ mm in the subsequent simulation.

Meanwhile, choosing the appropriate m value in the system is very important, as a large m will cause big static deformation of the diaphragm, while a small m can limit the sensitivity of the accelerometer. In COMSOL software, set $w = [1.0, 3.0]$ (unit: mm), $m = [7.1, 10.25]$ (unit: g), Fig. 5(a) shows the corresponding system resonant frequency obtained from the simulation, which gradually increases with the increase of w and decrease of m . Similarly, at a fixed beam length, the system has multiple sets of m and w values corresponding to the same resonant frequency. Selecting 636 Hz as the resonant frequency of the system in interest, the effect of the structural parameters including m as well as w on the sensitivity of the system was investigated. From Fig. 5(b), it can be seen that the system sensitivity is highest for $w = 2$ mm and $m = 7.1$ g in the selected parameter range.

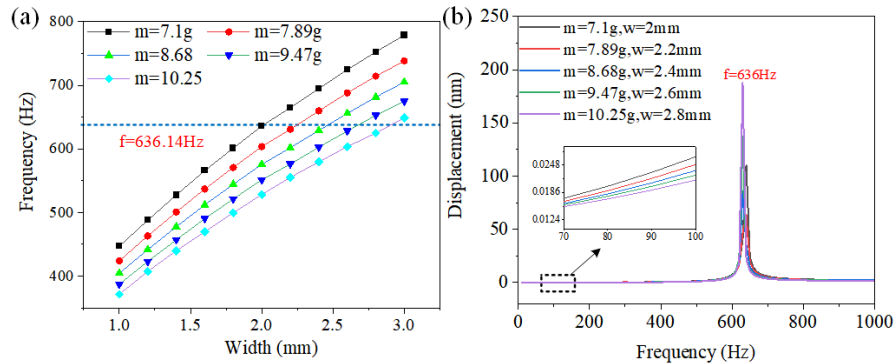


Fig. 5. Elastic diaphragm and mass structure simulation results 2. (a) Simulation of resonant frequency for different masses and crossbeam widths. (b) Simulation of the stress sensitivity of the structure at the same resonance frequency with different parameters, the insert is an enlarged picture of part of the area.

3. Experiment results and discussion

3.1. Fabrication

Based on the above simulation results, an acceleration sensor was fabricated by the laser cutting method, as shown in Fig. 6. The Qbe2 metal sheet with a thickness of 0.3 mm was used for fabricating the elastic diaphragm with crossbeam structure. The width of the crossbeam is 2 mm and the length of the crossbeam is 6 mm. As shown in Fig. 6(a), the mass block with a weight of 7.1 g was fixed onto the elastic diaphragm using a reliable optical adhesive (NOA68, Thorlab, USA). An FBG with a central wavelength of 1541.89 nm, a reflectivity of 86.93% and a bandwidth of 0.4 nm was used for acceleration measurements. The effective length of the FBG is about 10 mm. One end of the FBG is fixed inside the mass block by using the optical adhesive through the hole in the center of the mass block, the other end is placed outside the sensor through the hole at the bottom of the metal shell. Noted that the grating area of the FBG is all located inside the metal shell as shown in Fig. 2(c). Figure 6(b) shows the picture of the tail of the sensor. For acceleration measurements, the FBG needs to be pre-stretched to ensure that the FBG has a linearly strain response. The sensor package structure is shown in Fig. 6(c), the length of the sensor is 47 mm and the width is 28 mm, which can be easy to be mounted on vibration surface.

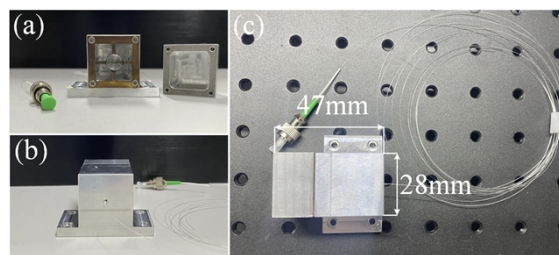


Fig. 6. Sensor physical photos. (a) Sensor internal structure. (b) Sensor tail structure. (c) Sensor photo and dimensioning.

3.2. Experimental setup

As shown in Fig. 7, a vibration detection system was built to measure the linear response of the designed FBG accelerometer. The FBG accelerometer is fixed on the surface of the shaker, and

a computer-controlled shaker can realize one-dimensional vibration with different frequencies and accelerations. An FBG wavelength interrogator was developed whose operating principle is based on the spectrum method, as shown in Fig. 8. An amplified spontaneous emission (ASE) light source is used, and the light transmits into a circulator and 1×N optical fiber coupler. The light is reflected by FBG sensors and the reflected light is then demodulated by the diffraction gratings. The interrogator has a demodulation frequency of up to 10 kHz.

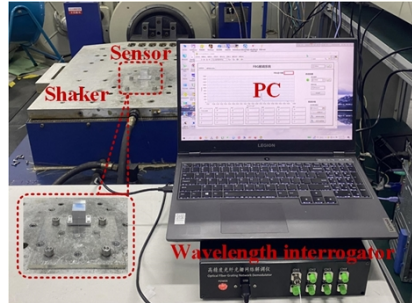


Fig. 7. Vibration detection system including PC, wavelength interrogator, shaker and accelerometer.

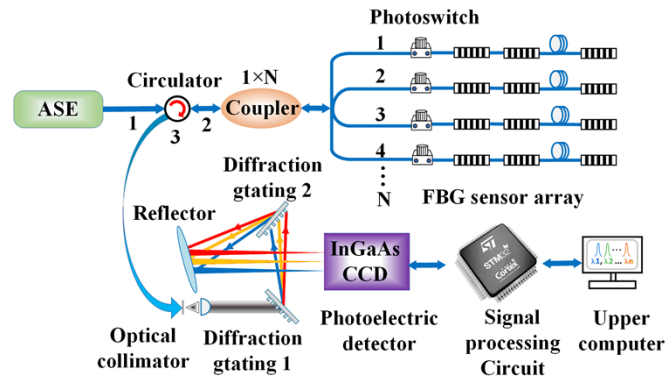


Fig. 8. The Composition and working principle of diffraction grating-based wavelength interrogator.

The stability was verified by the FBG wavelength interrogator set at a demodulation rate of 1 Hz, by recording the variation of the central wavelength of the sensor at rest over a period of 5 hours. As shown in Fig. 9(a), the recorded central wavelength is very stable. Figure 9(b) shows the histogram of the central wavelength distribution during the test, indicating that the FBG central wavelength is concentrated in the range of (1541.890 ± 0.001) nm. The test results show that the designed sensor has excellent stability.

3.3. Experimental results and discussion

In the experiments, the shaker was controlled to output a sinusoidal excitation with a vibration frequency ranging from 10 Hz to 500 Hz when the vibration acceleration is set at 1 g ($1 \text{ g} = 9.8 \text{ m/s}^2$). The time response waveforms of the sensor under different frequency excitation are observed and plotted as Fig. 10(a). It can be observed that the time domain response waveform of the sensor is smooth and clear. Figure 10(b) shows the amplitude-frequency response curve of the sensor.

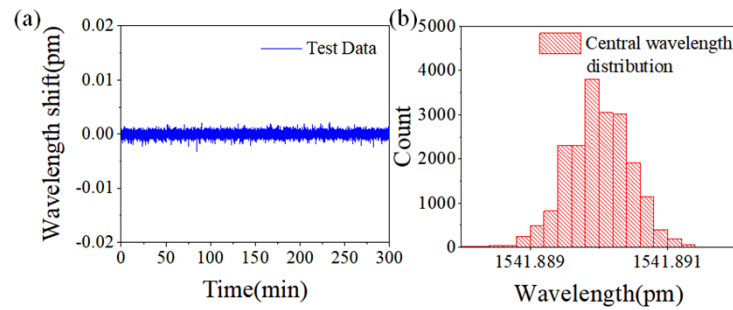


Fig. 9. Stability testing of sensors at rest. (a) Central wavelength shift of the sensor obtained by demodulation in 300 minutes. (b) Histogram of central wavelength distribution in (a).

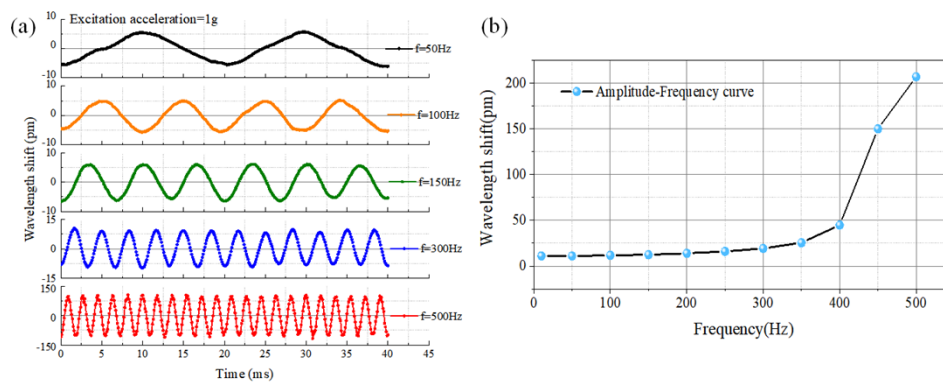


Fig. 10. (a) Time domain response waveform of changing vibration frequency to 50, 100, 150, 300, 500 Hz at vibration acceleration = 1 g. (b) The frequency response of the sensor when the vibration frequency is gradually increased from 10 Hz to 500 Hz at 1 g acceleration.

Typically, a flat response region is used as the working region of the sensor, which is in the frequency range of 10-200 Hz. Noted that the wavelength shift increases as the frequency increases, and the maximal shift is obtained when the frequency is near at 500 Hz, which indicates that this frequency is close to the resonant frequency of the sensor. In order to further investigate the resonant frequency of the sensor, a shock test is applied. Figure 11(a) shows the time domain response signal of the accelerometer when the free shock force is applied. After FFT transformation, the frequency response of the self-excited vibration is shown in Fig. 11(b). The resonant frequency of the accelerometer is about 556.645 Hz, which is basically consistent with the resonant frequency based on theoretical calculation. The difference in resonant frequencies may be induced by the improper manufacturing process, and additionally, the mass block is not integrated with the elastic diaphragm, which could lead to variations and shift the resonant frequency.

In order to investigate the linear response capability of the sensor to acceleration, vibration acceleration response tests were performed. During the test, the frequency of the sinusoidal excitation signal was fixed at 100 Hz and 150 Hz, the vibration acceleration of the shaker was set to increase from 0.6 to 6 g with a step of 0.6 g, and the wavelength shift of the sensor under different accelerations was recorded using the FBG wavelength interrogator. Figure 12 shows the time response of the sensor at several typical vibration acceleration during the test, from which it can be seen that the offset of the FBG center wavelength increases linearly as the vibration acceleration increases.

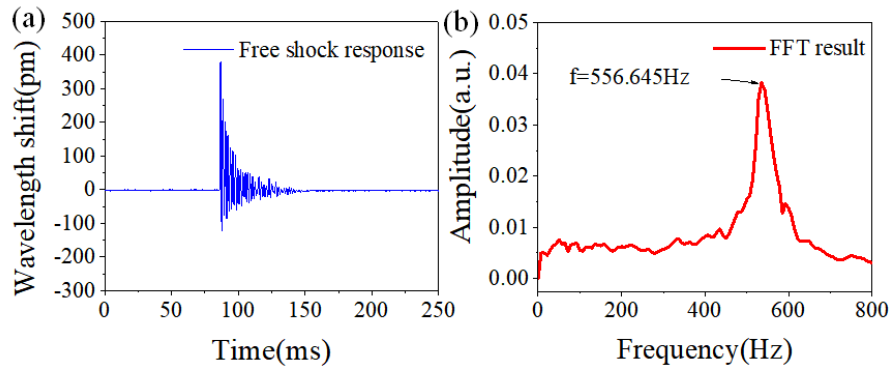


Fig. 11. Sensor free shock response experiment. (a) Free shock response time domain signal. (b) FFT calculation results of (a).

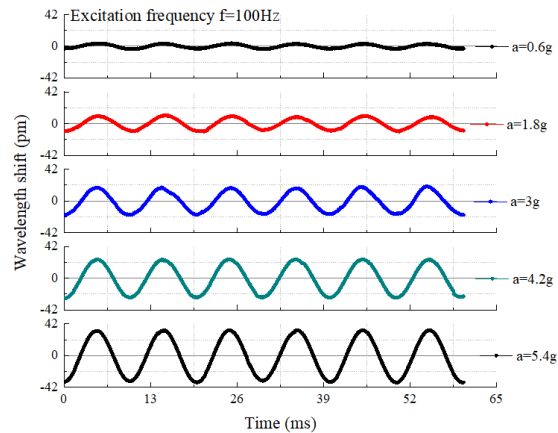


Fig. 12. The time domain response waveform of the sensor under different accelerations at the vibration frequency $f = 100\text{ Hz}$

The experiments were repeated for several times and the amplitude versus acceleration at 100 Hz and 150 Hz are plot as shown in Fig. 13. The acceleration sensitivity is about 12.35 pm/g, and the linear sensitivity of the sensor is 0.999. Considering that the FBG interrogator used has a measurement resolution of 0.5 pm, we can obtain a minimal resolution of 0.0404 g.

Since the designed accelerometer is a typical one-dimensional accelerometer, its immunity to vibrations in non-operating directions is of concern. In the experiment, the excitation frequency is kept at 100 Hz and the excitation acceleration is set to 1.2 g, 2.4 g, 3.6 g, 4.8 g, and 6 g, respectively, the time domain response in the work and non-work directions are obtained as shown in Fig. 14(a). It can be observed that the wavelength shift is quite small and the waveform is flat when the vibration occurs in the non-operating direction of the sensor, while the wavelength shift increases significantly when the vibration is in the operating direction. The linear responses of the sensor in the working and non-working directions are plotted as shown in Fig. 14(b). The maximal cross-error is calculated less than 3.26%, which implies that the sensor is highly immune to vibrations in the non-operating direction. Additionally, a comparison study between our work and the other reported work based on fiber grating sensors is displayed in Table 1. The results show that the sensing system has good stability compared to some of the current works. The presented work does not show a high sensitivity but it presents a flat response region in the range of 10-200 Hz. It should be noted that this can be significantly improved by optimizing

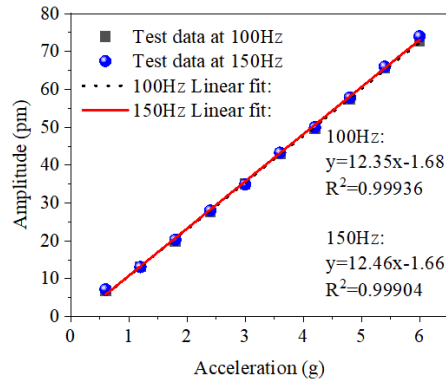


Fig. 13. The linear response test of sensor acceleration when the vibration frequency is $f = 100\text{ Hz}$ and 150 Hz , respectively.

the structural parameters. Meanwhile the proposed sensor shows ability for large acceleration sensing.

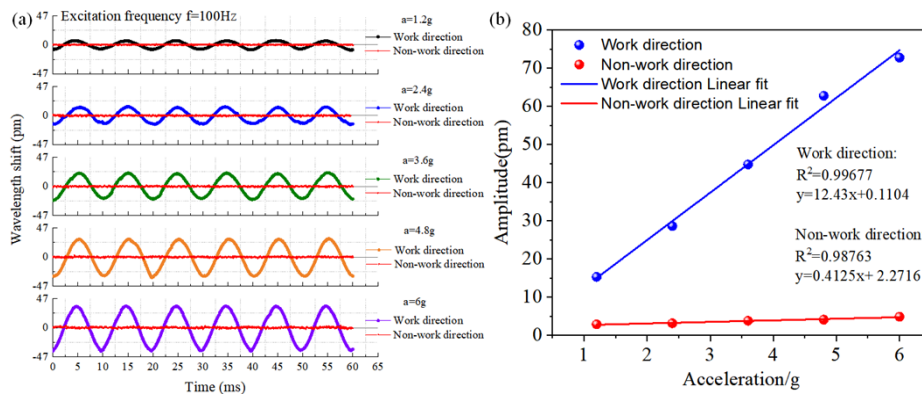


Fig. 14. Sensor cross sensitivity experiment (a) The time domain response of the sensor when vibration occurs in the work direction and non-work direction of the sensor at a vibration frequency of 100 Hz . (b) The linear response of sensor acceleration in work and non-work directions.

Table 1. Comparison between our work and other reported schemes

Authors	Sensing method	Resonance frequency	Bandwidth	Anti-interference	Sensitivity
Jiang at al. [17]	FBG	119 Hz	2-60 Hz	<3.86%	143.29 pm/g
Liu at al. [19]	FBG	41 Hz	4-30 Hz	<3.89%	85.8 pm/g
Weng at al. [31]	FBG	170 Hz	10-120 Hz	<5%	100 pm/g
Liu at al. [32]	FBG	103 Hz	1-60 Hz	<5%	754.3 pm/g
This work	FBG	556 Hz	10-200 Hz	<3.26%	12.35 pm/g

4. Conclusion

In this work, a spring-mass structure-based FBG accelerometer was proposed, fabricated and tested. The resonant frequencies of the acceleration systems with different diaphragm sizes and

mass blocks were investigated and optimized to achieve a high sensitivity. The experimental results showed that the device has a resonant frequency of 556.645 Hz and a flat response region in the range of 10-200 Hz. The acceleration sensing sensitivity is 12.35pm/g. Due to the strong anti-interference (maximum cross-error less than 3.26%), the proposed device could be a good choice for one-dimensional accelerometer. In future works, some temperature compensation techniques will be considered as to better highlight the high stability of the sensor.

Funding. National Key Research and Development Program of China (2023YFB3209500); National Natural Science Foundation of China (62375237); Natural Science Foundation of Shanghai Municipality (20ZR1420300); Yangtze River Delta Community of Sci-Tech Innovation Field Program (23002400300); Fundação para a Ciência e a Tecnologia (LA/P/0006/2020, PTDC/EEI-EEE/0415/2021, UIDB/50011/2020, UIDP/50011/2020).

Acknowledgments. This work was developed within the scope of the projects CICECO (LA/P/0006/2020, UIDB/50011/2020 & UIDP/50011/2020) and DigiAqua (PTDC/EEI-EEE/0415/2021), financed by national funds through the (Portuguese Science and Technology Foundation/MCTES (FCT I.P.)). This work was co-funded by the financial support of the European Union under the REFRESH – Research Excellence For REgion Sustainability and High-tech Industries project number CZ.10.03.01/00/22_003/0000048 via the Operational Programme Just Transition as well as supported by grants SP2024/059 and SP2024/081 (FEECS, VSB -Technical University of Ostrava, Czech Republic).

Disclosures. The authors declare no conflicts of interest.

Data availability. Data underlying the results presented in this paper are not publicly available at this time but may be obtained from the authors upon reasonable request.

References

1. S. Xu, F. Xing, R. Wang, *et al.*, “Vibration sensor for the health monitoring of the large rotating machinery: review and outlook,” *Sensor Rev.* **38**(1), 44–64 (2018).
2. J. Ding, “Fault detection of a wheelset bearing in a high-speed train using the shock-response convolutional sparse-coding technique,” *Measurement*. **117**, 108–124 (2018).
3. X. Qiao, Z. Shao, W. Bao, *et al.*, “Fiber Bragg grating sensors for the oil industry,” *Sensors* **17**(3), 429 (2017).
4. C. Hong, Y. Zhang, M. Zhang, *et al.*, “Application of FBG sensors for geotechnical health monitoring, a review of sensor design, implementation methods and packaging techniques,” *Sens. Actuators, A* **244**, 184–197 (2016).
5. X. W. Ye, Y. H. Su, and J. P. Han, “Structural health monitoring of civil infrastructure using optical fiber sensing technology: a comprehensive review,” *The Scientific World J.* **2014**, 1–11 (2014).
6. F. Zhang, Z. Yuan, F. Zhang, *et al.*, “The analysis and estimation of vibration fatigue for pipe fitting in aviation hydraulic system,” *Eng. Fail. Anal.* **105**, 837–855 (2019).
7. D. P. Connolly, G. Kouroussis, O. Laghrouche, *et al.*, “Benchmarking railway vibrations – Track, vehicle, ground and building effects,” *Constr. Build. Mater.* **92**, 64–81 (2015).
8. H. Wei, C. Tao, Y. Zhu, *et al.*, “Fiber Bragg grating dynamic strain sensor using an adaptive reflective semiconductor optical amplifier source,” *Appl. Opt.* **55**(10), 2752–2759 (2016).
9. Z. Shen, C. Y. Tan, K. Yao, *et al.*, “A miniaturized wireless accelerometer with micromachined piezoelectric sensing element,” *Sens. Actuators, A* **241**, 113–119 (2016).
10. S. K. Reguieg, Z. Ghemari, T. Benslimane, *et al.*, “Modeling and Enhancement of Piezoelectric Accelerometer Relative Sensitivity,” *Sens. Imaging*. **20**(1), 1 (2019).
11. M. M. Khan, N. Panwar, and R. Dhawan, “Modified cantilever beam shaped FBG based accelerometer with self temperature compensation,” *Sens. Actuators, A* **205**, 79–85 (2014).
12. J. M. Lopez-Higuera, L. R. Cobo, A. Q. Incera, *et al.*, “Fiber optic sensors in structural health monitoring,” *J. Lightwave Technol.* **29**(4), 587–608 (2011).
13. F. Marignetti, E. Santis, S. Avino, *et al.*, “Fiber Bragg grating sensor for electric field measurement in the end windings of high-voltage electric machines,” *IEEE Trans. Ind. Electron.* **63**(5), 2796–2802 (2016).
14. T. Li, J. Guo, Y. Tan, *et al.*, “Recent advances and tendency in fiber Bragg grating-based vibration sensor: a review,” *IEEE Sens. J.* **20**(20), 12074–12087 (2020).
15. H. Wei, X. Zhao, D. Li, *et al.*, “Corrosion monitoring of rock bolt by using a low coherent fiber-optic interferometry,” *Opt. Laser Technol.* **67**, 137–142 (2015).
16. N. Basumallick, I. Chatterjee, P. Biswas, *et al.*, “Fiber Bragg grating accelerometer with enhanced sensitivity,” *Sens. Actuators, A* **173**(1), 108–115 (2012).
17. L. Jiang, D. Yu, H. Gao, *et al.*, “A fiber Bragg grating accelerometer with cantilever beam,” *Opt. Fiber Technol.* **74**, 103088 (2022).
18. W. Fan, J. Wen, H. Gao, *et al.*, “Low-frequency fiber Bragg grating accelerometer based on diaphragm-type cantilever,” *Opt. Fiber Technol.* **70**, 102888 (2022).
19. Q. Liu, Z. Jia, H. Fu, *et al.*, “Double cantilever beams accelerometer using short fiber Bragg grating for eliminating chirp,” *IEEE Sens. J.* **16**(17), 6611–6616 (2016).
20. B. Yan and L. Liang, “A novel fiber Bragg grating accelerometer based on parallel double flexible hinges,” *IEEE Sens. J.* **20**(9), 4713–4718 (2020).

21. L. Qiu, L. Liang, D. Li, *et al.*, “Theoretical and experimental study on FBG accelerometer based on multi-flexible hinge mechanism,” *Opt. Fiber Technol.* **38**, 142–146 (2017).
22. G. Yin, Y. Dai, J. Karanja, *et al.*, “Optimization design for medium-high frequency FBG accelerometer with different eigenfrequency and sensitivity,” *Sens. Actuators, A* **235**, 311–316 (2015).
23. Q. Liu, X. Qiao, Z. A. Jia, *et al.*, “Large frequency range and high sensitivity fiber bragg grating accelerometer based on double diaphragms,” *IEEE Sens. J.* **14**(5), 1499–1504 (2014).
24. X. Wang, Y. Guo, L. Xiong, *et al.*, “High-frequency optical fiber bragg grating accelerometer,” *IEEE Sens. J.* **18**(12), 4954–4960 (2018).
25. J. Zhu, J. Wang, P. Gan, *et al.*, “Design and analysis of a novel dual FBG accelerometer based on lantern shape metallic shells,” *IEEE Sens. J.* **17**(16), 5130–5135 (2017).
26. T. Li, C. Shi, Y. Tan, *et al.*, “A diaphragm type fiber Bragg grating vibration sensor based on transverse property of optical fiber with temperature compensation,” *IEEE Sens. J.* **17**(18), 5840–5848 (2017).
27. Q. P. Liu, X. G. Qiao, J. L. Zhao, *et al.*, “Novel Fiber Bragg Grating Accelerometer Based on Diaphragm,” *IEEE Sens. J.* **12**(10), 3000–3004 (2012).
28. A. Leal-Junior, A. Frizera, and C. Marques, “A fiber gratings pair embedded in a polyurethane diaphragm: Towards a temperature-insensitive pressure sensor,” *Opt. & Laser Technol.* **131**, 106440 (2020).
29. A. Leal-Junior and C. Marques, “Diaphragm-embedded optical fiber sensors: a review and tutorial,” *IEEE Sens. J.* **21**(11), 12719–12733 (2021).
30. J. Chen, T. Chang, Y. Yang, *et al.*, “Ultra-low-frequency tri-component fiber optic interferometric accelerometer,” *IEEE Sensors J.* **18**(20), 8367–8374 (2018).
31. Y. Weng, X. Qiao, T. Guo, *et al.*, “A robust and compact fiber Bragg grating vibration sensor for seismic measurement,” *IEEE Sens. J.* **12**(4), 800–804 (2012).
32. Q. Liu, W. Liu, C. Wang, *et al.*, “High figure of merit and low cross sensitivity fiber Bragg grating accelerometer based on double grid-diaphragms,” *IEEE Sens. J.* **21**(24), 27503–27509 (2021).